Research

Effect of the thickness on the photocatalytic and the photocurrent properties of ZnO films deposited by spray pyrolysis

A. Sulthan Ibrahim[1] · Kevin V. Alex[1] · M. Bhakya Latha[2] · K. Kamakshi[2] · S. Sathish[3] · J. P. B. Silva[4,5] · K. C. Sekhar[1]

Abstract

In this work, we have investigated the structure, morphology, photoluminescence, photocatalytic and photocurrent properties of ZnO thin films as a function of their film thickness (t_{ZnO}) fabricated via ultrasonic spray pyrolysis technique. The X-Ray diffraction patterns exhibited the formation of polycrystalline wurtzite phase of ZnO. Scanning electron microscopy images showed the uniform morphology with nanorod structure. The photosensitivity and photocatalytic efficiency are found to be optimum at $t_{ZnO} = 1200$ nm and are attributed to the improved photogeneration of charge carriers and higher concentration of oxygen vacancies. A direct correlation is established between the photosensitivity and photo-degradation process. The incident photon-to-electron conversion efficiency (IPCE) and photocatalytic efficiency for the ZnO film at $t_{ZnO} = 1200$ nm are estimated to be 31.5% and 100% respectively. The obtained result suggests that ZnO thin films are potential candidates for applications in various optoelectronic devices.

Keywords Ultrasonic spray pyrolysis · ZnO · Photoluminescence · I-V characteristics · Photocatalytic

1 Introduction

Nowadays, the demand for research drives the significant focus on materials with unique properties for wide applications. Therefore, the prime aim of the research fraternity is to address these issues effectively. In such a scenario, zinc oxide (ZnO) can be foreseen as an efficient electronic, optical and energy material with negligible environmental contamination [1]. It is well-known that ZnO is a direct bandgap (3.4 eV) semiconductor, with a large exciton binding energy of 60 meV and excellent thermal/mechanical stability. It has grabbed the wide attention of the scientific community due to its versatile electronic/optical properties towards the various applications. Particularly, optical studies on ZnO thin film are essential for the utilization in optoelectronic devices. In general, optical properties of ZnO can be tuned by varying microstructure, thickness, bandgap energy, optically active defects and growth/deposition conditions [2]. So far ZnO has been reported as one of the efficient materials for photocatalysis and photovoltaic because of its tuneable properties with low cost and non-toxicity [3, 4].

Tremendous research work has been focussing on tuning the properties of ZnO thin films; thereby preparation methods are playing a crucial role to tune the properties of the material to attain the utilization of ZnO thin film in the desired

✉ J. P. B. Silva, josesilva@fisica.uminho.pt; ✉ K. C. Sekhar, sekhar.koppole@gmail.com | [1]Department of Physics, Central University of Tamil Nadu, Thiruvarur 610 005, India. [2]Department of Physics, Indian Institute of Information Technology (IIIT), Trichcurappalli, Tamil Nadu, India. [3]Department of Physics, MVJ College of Engineering, Bangalore 560 067, India. [4]Centre of Physics of Universities of Minho and Porto (CF-UM-UP), Campus de Gualtar, 4710-057 Braga, Portugal. [5]Laboratory of Physics for Materials and Emergent Technologies, LapMET, University of Minho, 4710-057 Braga, Portugal.

Springer

applications. Saravanan et al. compared the photocatalytic activity of nanosized ZnO prepared by different methods such as thermal decomposition, precipitation and sol–gel process [5]. They have observed that the ZnO prepared via the sol–gel process exhibited a higher efficiency of 99% in 120 min of UV illumination for the degradation of methylene blue (MB) dye in comparison with the ZnO synthesized through other methods. Recently in 2021, Uribe-Lopez et al. compared the photocatalytic activity of ZnO nanoparticles prepared via precipitation and sol–gel method [6]. ZnO prepared via precipitation method exhibited an excellent efficiency of 100% in 120 min of UV illumination for phenol degradation when compared with that of ZnO prepared via sol–gel technique (80%). Kaneva et al. compared the photocatalytic activity of ZnO thin film fabricated via spray pyrolysis and sol–gel technique [7]. The ZnO film fabricated via spray pyrolysis at 350 °C exhibited an improved efficiency of 68.8% in 180 min of UV irradiation than that for the sol–gel prepared ZnO film (59.8%) for the degradation of malachite green (MG) dye. Furthermore, Klauson et al. fabricated ZnO nanostructured layers with various morphologies via the spray pyrolysis technique and the needle-like ZnO structure was observed to be more efficient for photocatalytic degradation of humic acid (HA) [8]. Nowadays, new methods/technology involves in developing cheaper and flexible devices. Indeed, thin film technology is playing a prime role to obtain the enhanced properties with defect-free thin films suitable to the electronic and optoelectronic devices. The existing ZnO thin films have been fabricated by various deposition techniques such as spin coating, dip coating, spray pyrolysis, ultrasonic spray pyrolysis, sputtering, pulsed laser deposition, hydrothermal method, electrochemical deposition, etc. [9–13]. Among these, the ultrasonic spray pyrolysis technique can be seen as a low-cost as well as an effective technique for the fabrication of uniform and large-area film coatings with minimal chemical wastage [11, 14].

It is known that film thickness critically affects the crystal structure as well as the morphology of the photocatalysts. Recently, Bakhtiarnia and co-workers studied the effect of the film thickness of sputtered $BiVO_4$ films on their structural, morphological, optical and photocatalytic properties and found that the efficiency was optimum at a thickness of 715 nm [15]. The film thickness can play a vital role in the generation and transport of charge carriers, which in turn affect the photovoltaic and photocatalytic performances. Pianaud et al. studied that the film thickness of Ta_3N_5 films has a crucial impact on the charge generation and transport mechanism [16]. The photoactivity and incident photon-to-current efficiency (IPCE) is found to be higher for thicker films than for thinner ones. Various works have studied the photocatalytic and photocurrent properties of ZnO separately, but only a few works have reported the correlation between the two. Even though various works have reported excellent efficiency of ~100% for ZnO, it is essential to decrease the photocatalytic reaction time (illumination time) in order to improve its photocatalytic activity for commercial employability [5, 6]. Hence, in this work we are trying to enhance the photocatalytic activity of ZnO film further. We have reported on ZnO thin films as a function of their thickness (t_{ZnO}) to explore the photocatalytic and photocurrent properties in a vivid manner. Thus, this work highlights the multidimensional employability of low-cost ZnO thin films fabricated as a function of their thickness in various optoelectronic device applications.

2 Experimental

2.1 Preparation of ZnO thin films

The precursor solution was prepared as per the stoichiometric ratio as follows. 2.1950 g of zinc acetate dehydrate ($ZnCH_3COO_2$)0.2H_2O (MERCK) and 4 ml of acetic acid glacial (CH_3COOH) (MERCK) were added with 100 ml of deionized water. The mixture was stirred for one hour on a magnetic stirrer at 65 °C at 500 rpm. Meanwhile, the ultrasonic spray deposition nebulizer (OMRON NE-U780) was carefully cleaned and the prepared sol was transferred to the cup of the nebulizer after one hour of stirring. The nebulization rate and airflow volume were set at 3 ml/min and 17 L/min. The average aerosol output rate was 0.14 ml/min. Pre-cleaned glass plates were used as the substrate and were placed on the hot plate at a temperature of 400 °C. ZnO films were deposited on the glass substrates with different spray timings and were annealed at 400 °C for 2 h. The thickness of ZnO films (t_{ZnO}) is varied from 80 to 1200 nm.

2.2 Characterization of ZnO thin films

The microstructure of ZnO films was studied using an X-ray diffractometer (Malvern Panalytical system) in the range of 25°–60° with a step size of 0.008° using the Cu Kα radiation with a wavelength of 0.154 nm. The surface morphological studies were done using by SEM instrument (Carl ZEISS). The photoluminescence spectra of the films were recorded using the Perkin Elmer L55 fluorescence spectrometer at an excitation wavelength of 340 nm. To study

the current–voltage characteristics (I-V), the ZnO thin films were deposited over conductive ITO substrates in parallel plate electrode configuration with Ag as the top electrode and ITO as the bottom electrode. The Ag electrodes were deposited via DC sputtering technique.The photocurrent of the ZnO thin films was measured using a white light LED source with wavelength range of 400–800 nm with a measured power density of 15 W/m^2. Similarly, the incident photon-to-electron conversion efficiency (IPCE) factor was studied using a monochromatic red-light source with a measured power density of 20 W/m^2. The photocatalytic activity of the ZnO thin films was studied using 0.5 mM Rhodamine B (RhB) aqueous dye solution as a template under halogen lamp illumination (wavelength range: 350–1000 nm) of 15 min. Furthermore, the time dependence, as well as the reusability of the ZnO thin film photocatalysts, were also determined.

3 Results and discussions

3.1 Structural studies

The X-ray diffraction patterns of ZnO thin films deposited at different ZnO thicknesses (t_{ZnO}) are shown in Fig. 1. The diffraction peaks (100), (002), (101) and (110) indicated the formation of polycrystalline wurtzite phase of ZnO (ICSD. 01-078-4603) without any secondary or impurity phase [29]. It is observed that the intensity of (100), (002) and (101) diffraction peaks increase with the increase of t_{ZnO} indicating the continuous growth of ZnO layers. The growth rate along the (002) orientation is observed to be lower than that of the (100) and (101) orientations because of its higher surface energy [17, 18].

Usually, the exposed (002) plane has a polar surface and thus induces dipole nature with the positive Zn-terminated (002) facets and negative O-terminated (00-2) facets. The Zn^{+2} ionic sites on the (002) facets have a great affinity towards oxygen adsorption and results in the capture of electrons near the surface and hence forms a thin layer of O_2^- on the ZnO surface. This surface space charge region can act as a hole trapping center and thus enhance the charge carrier separation [18, 19].The surface polarity of ZnO films can be estimated by taking the intensity ratio (I_{002}/I_{100}) and is tabulated in Table 1. But, in this work, it is observed that this ratio is decreased as t_{ZnO} increased from 240 to 1200 nm and it can be attributed to the lower growth rate along (002) orientation [18, 20]. Furthermore, the higher amount of unsaturated Zn^{2+} along (100) facet improves the adsorption of oxygen-containing species and favours the formation of reactive radicals which aids in the photocatalytic mechanism [21].The crystal lattice parameters and crystallite size of the ZnO films were also estimated and are tabulated in Table 1. The lattice parameters were estimated by using the standard formula for the hexagonal crystal lattice given as;

Fig. 1 XRD pattern of ZnO thin films deposited at different t_{ZnO}
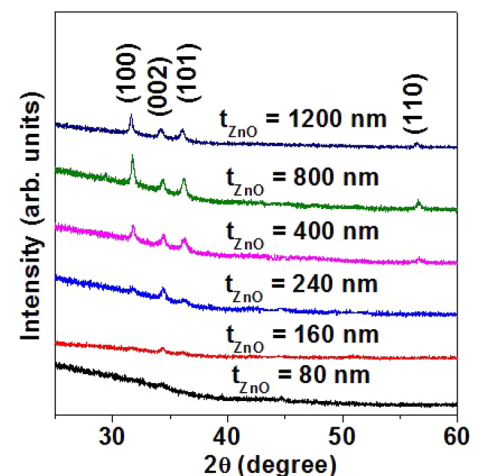
Table 1 Lattice parameters and crystallite size of ZnO thin films at different t_{ZnO}

$t_{ZnO\,(nm)}$	I_{002}/I_{100}	$a = b$ (Å)	c (Å)	c/a	Crystallite size (nm)
80	–	–	–	–	–
160	–	$3.234 \pm 0.46\%$	$5.177 \pm 0.53\%$	1.600	37
240	1.73	$3.250 \pm 0.03\%$	$5.207 \pm 0.03\%$	1.602	36
400	0.75	$3.244 \pm 0.15\%$	$5.199 \pm 0.11\%$	1.602	36
800	0.42	$3.252 \pm 0.09\%$	$5.211 \pm 0.11\%$	1.602	65
1200	0.37	$3.264 \pm 0.46\%$	$5.219 \pm 0.26\%$	1.598	72

$$d_{(hkl)} = \frac{1}{\sqrt{\left(\frac{\frac{4}{2}\left(h^2 + hk + k^2\right)}{a^2} + \frac{l^2}{c^2} \right)}} \tag{1}$$

where 'a', 'b' and 'c' are the lattice parameters. The crystallite size was estimated using the Debye–Scherrer equation [18],

$$D = \frac{0.9\lambda}{\beta \cos\theta} \tag{2}$$

where 'λ' is the wavelength of the X-ray ($= 0.154$ nm) and 'β' is the full width at half maximum in radians. It is found that the crystallite size increases with the increase of t_{ZnO} which exhibits the growth of ZnO nanostructures.

3.2 Morphological studies

The SEM images of the ZnO thin films with different t_{ZnO} are shown in Fig. 2a–e. SEM images showed the uniform morphology with nanorod structure. It is also seen that the grains are uniformly distributed over the entire film surface. The density of grains is found to be increasing with the increase of t_{ZnO}. It is in good agreement with the fact that growth rate
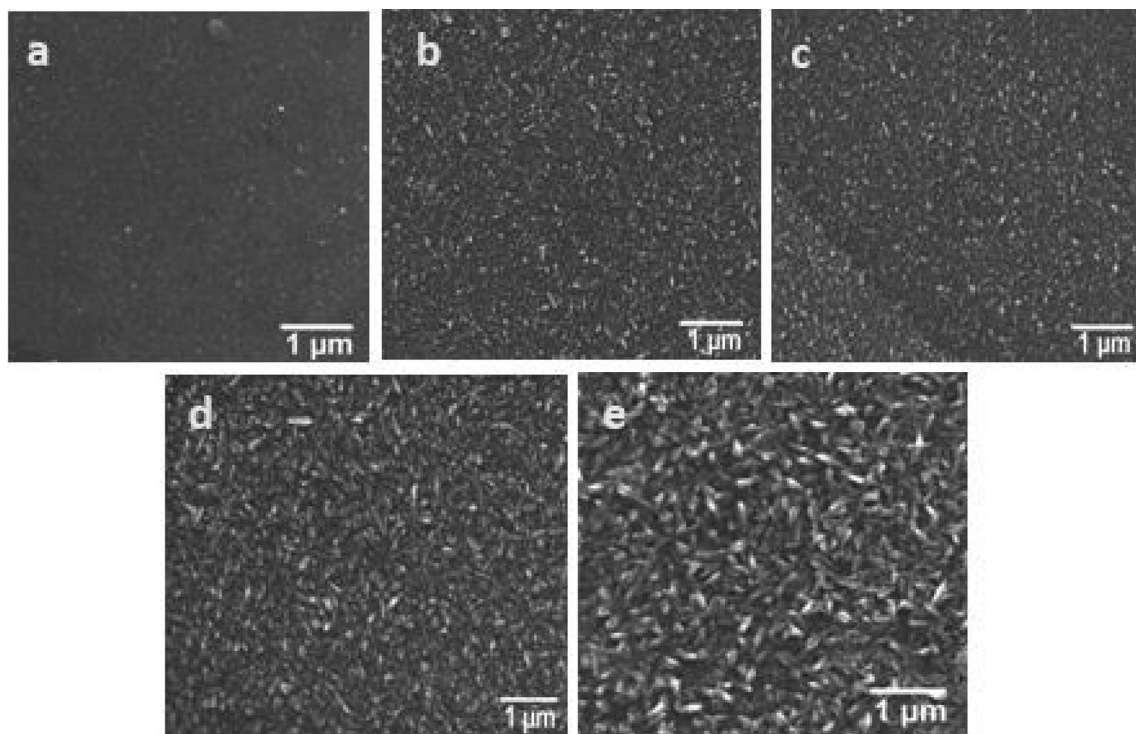
Fig. 2 SEM images of ZnO thin films at **a** $t_{ZnO} = 80$ nm **b** $t_{ZnO} = 240$ nm **c** $t_{ZnO} = 400$ nm **d** $t_{ZnO} = 800$ nm **e** $t_{ZnO} = 1200$ nm

(grains) increases as increase of film thickness of ZnO thin films [22, 23]. The increase in the particle size and density of ZnO grains with the increase of t_{ZnO} can improve the photogeneration and separation of charge carriers [24]. Moreover, the aspect ratio (length to width ratio) of the ZnO nanostructures is found to be increased with the increase of t_{ZnO} as tabulated in Table 2. A higher aspect ratio favours photocatalytic activity and found to be higher at $t_{ZnO} = 1200$ nm [21].

3.3 Optical studies

The transmittance spectra of the ZnO films deposited at different t_{ZnO} is depicted in Fig. 3a. The red shift observed in the fundamental absorption edge illustrates the decrease in bandgap energy with t_{ZnO}. The decrease in bandgap energy with the increase in particle size confirmed the quantum size confinement effect [5]. The optical bandgap energy is estimated using the well-known Tauc plot as shown in Fig. 3b and is tabulated in Table 3. It is found to be minimum at $t_{ZnO} = 1200$ nm. A lower bandgap enables a higher absorption of light and thus can improve the photogeneration of charge carriers [15].

The photoluminescence spectra of the ZnO films deposited at different t_{ZnO} at an excitation wavelength of 340 nm are shown in Fig. 4a.The peak positions in PL spectrum were determined for all films by using the multi-peak Gaussian fit in origin software and the typical one is shown in Fig. 4b. All the films exhibited one emission peak in the UV region and four other emission peaks in the visible region. The observed UV emissions are due to band-to-band transitions

Table 2 Dimensions and aspect ratio of the ZnO nanostructures

| t_{ZnO} (nm)	Length (nm)	Width (nm)	Aspect ratio
80	$72 \pm 7\%$	$64 \pm 10\%$	1.12
240	$98 \pm 9\%$	$85 \pm 18\%$	1.15
400	$100 \pm 12\%$	$83 \pm 15\%$	1.20
800	$186 \pm 18\%$	$127 \pm 16\%$	1.46
1200	$216 \pm 10\%$	$131 \pm 10\%$	1.64

Fig. 3 **a** Transmittance spectra of ZnO thin films deposited at different t_{ZnO}, **b** Tauc plot for the ZnO film with $t_{ZnO} = 1200$ nm
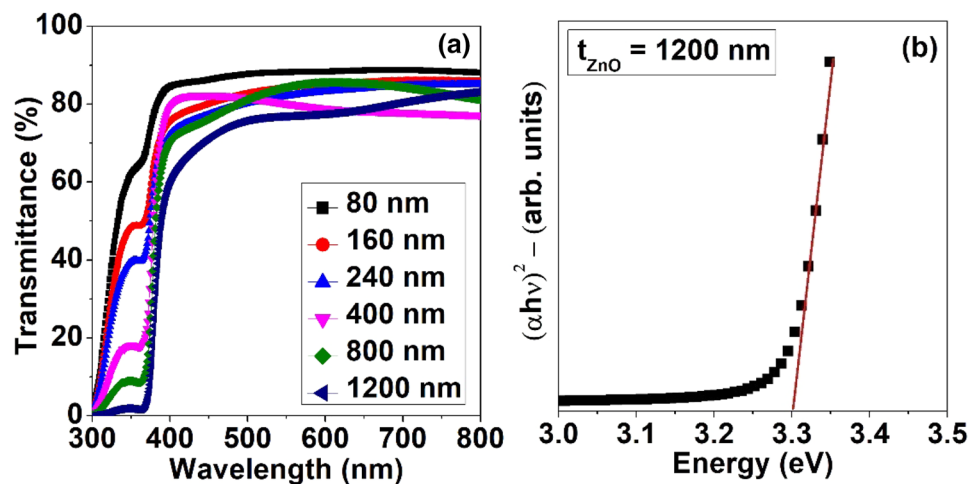
Table 3 Optical bandgap energy of ZnO thin films deposited at different t_{ZnO}

t_{ZnO} (nm)	Bandgap energy (eV)
80	3.51
160	3.46
240	3.41
400	3.38
800	3.34
1200	3.29

Fig. 4 **a** Photoluminescence spectra of ZnO thin films deposited at different t_{ZnO}, **b** Multi-peak Gaussian fitting for the PL spectra of ZnO film with $t_{ZnO} = 240$ nm, and **c** Ratio of oxygen vacancies to band-to-band transition as a function of t_{ZnO}
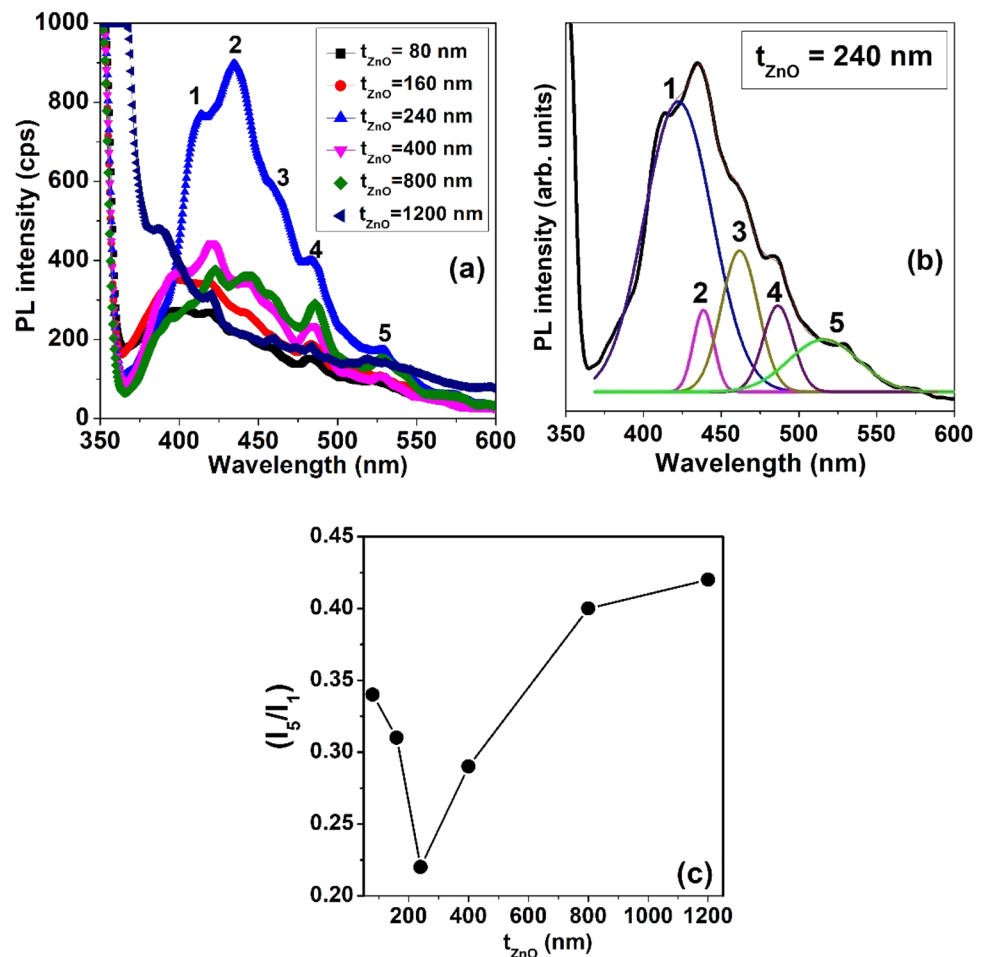

and visible emissions are due to the shallow defects and/or deep level defects [25]. Wang et al. reported that the non-radiative and radiative transition probabilities on ZnO which is attributed to crystal imperfection (point defects, grain boundaries and dislocations) for nonradiative transition whereas near band edge excitonic/deep level emission for radiative transition [26]. The observed emissions in the visible regions are due to the suppression of nonradiative defects such as point defects, grain boundaries and dislocations in the ZnO thin film. It also supports the defect-free ZnO film growth observed from SEM images.

The observed peak 1 at around 390 nm (UV emission) in the region can be attributed to the band-to-band transition [27].The observed peak 2 at around 420 nm (violet emission) is assigned to the transitions of electrons from zinc interstitials (Zn_i) to the valence band (VB). The observed peak 3 at around 460 nm (blue emission) is due to the transfer of an electron from conduction band (CB) to oxygen interstitials (O_i) while the observed peak 4 at around 480 nm (blue emission) arises due to the transition of electrons from Zn_i to zinc vacancies (V_{Zn}).The existence of green emission peak 5 at around 515 nm is due to the transition of electrons from the singly ionized oxygen vacancies (V_0^*) to VB. Oxygen vacancies play a predominant role than other crystal defects in the photocatalytic process [18]. The ratio of oxygen vacancies to band-to-band transition (I_5/I_1) is plotted as a function of t_{ZnO} and observed to be maximum at $t_{ZnO} = 1200$ nm as shown in Fig. 4c.

3.4 Current–voltage (I-V) characteristics

The current–voltage (I-V) characteristics of the ZnO films deposited at different t_{ZnO} from −1 to + 1 V under dark and light illumination conditions are plotted in Fig. 5a–d. The photocurrent values are increasing with the increase of bias voltage ranges observed for both dark and light illumination conditions. The observed increase in current after illumination is due to the increase in the number of mobile charge carriers and consequently the high electrical conductivity [28]. The observed increase in photocurrent value for higher thickness films is due to the increase of

**Fig. 5** I-V characteristics of ZnO thin films deposited at different t_{ZnO} under dark and light conditions
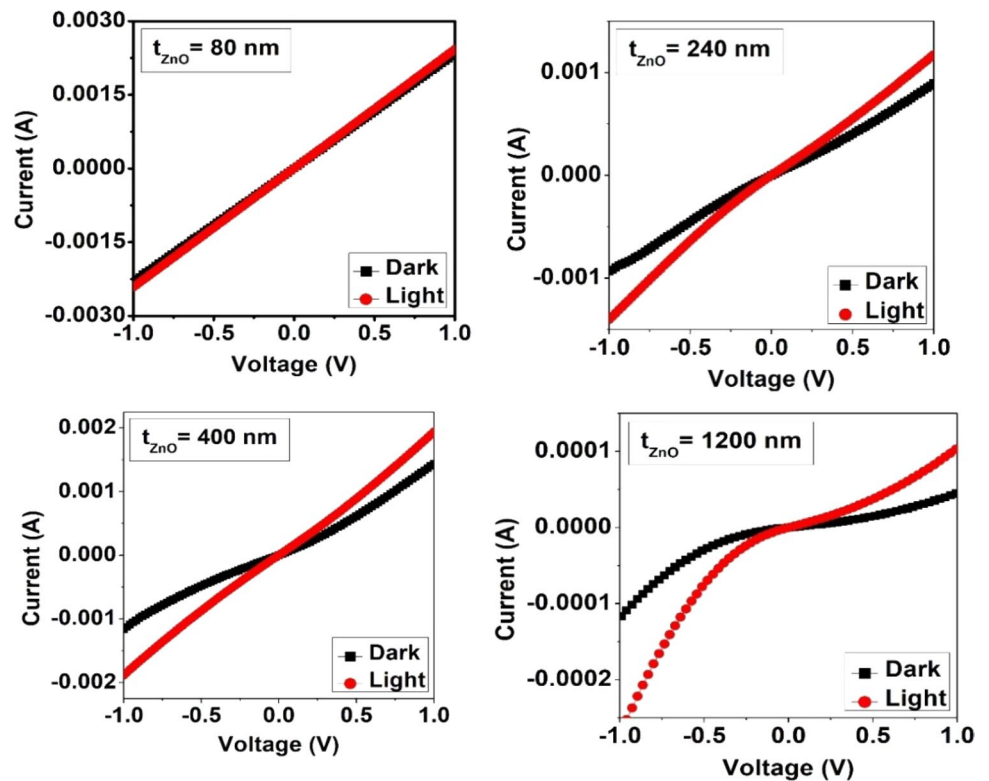
grain size and aspect ratio as evident from SEM images [21, 24, 29]. Photocurrent (I_{ph}) is defined as the difference of current under dark and light conditions at a specific voltage, i.e., $I_{ph} = I_{light} - I_{dark}$. The photosensitivity or photoresponse factor (S) as shown in Eq. (3), which is defined as the ratio of photocurrent (I_{ph}) to dark current (I_{dark}), is considered to be a crucial factor in determining the performance of photodetectors [30].

$$\text{Photosensitivity (S)} = \frac{I_{ph}}{I_{dark}} \qquad (3)$$

The photosensitivity at a voltage of 1 V estimated using Eq. 3 as a function of t_{ZnO} is as shown in Fig. 6. It is observed that the ratio of photosensitivity is increasing with an increase in t_{ZnO} and found to be maximum at $t_{ZnO} = 1200$ nm. The obtained results are good in accordance with the reported work on thickness-dependent ZnO-based semiconductor materials by various methods [28, 31–34]. This indicates the enhanced photogeneration of charge carriers at higher t_{ZnO}. Even though oxygen vacancies play a role in photocurrent generation, in this work, the thickness effect seems

Fig. 6 Photosensitivity of ZnO thin films as a function of t_{ZnO}
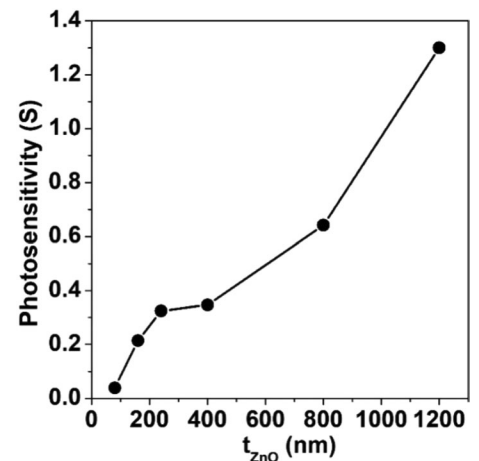
to have a dominant role over oxygen vacancies.The increase in the photogeneration of charge carriers concerning the increase in t_{ZnO} is evident from Fig. 6.

Since the ZnO film with $t_{ZnO} = 1200$ nm exhibited maximum photosensitivity, the incident photon-to-electron conversion efficiency (IPCE) factor of the film was also evaluated for photovoltaic device applications. IPCE is the ratio of the number of photogenerated charge carriers under short-circuit conditions to the number of incident photons at a particular wavelength and is a crucial parameter in the fabrication of photovoltaic devices. The IPCE efficiency is calculated using the following relation [35, 36].

$$IPCE = \frac{j_{ph}\left(\frac{mA}{cm^2}\right) \times 1239.8(V \times nm)}{P_{mono}\left(\frac{mW}{cm^2}\right) \times \lambda(nm)} \times 100 \qquad (4)$$

where 'j_{ph}' is the average steady-state photocurrent density, 'P_{mono}' and 'λ' is the optical power and wavelength of the incident monochromatic light source respectively. The IPCE for the ZnO film at $t_{ZnO} = 1200$ nm is estimated to be 31.5%. The photosensitivity of ZnO film with $t_{ZnO} = 1200$ nm under white light illumination and red-light illumination is 1.3 and 0.09 respectively. This clearly shows a much higher photocurrent generation under white light illumination than under red light illumination, as expected. The photocurrent under red illumination can be induced by the defects, especially oxygen vacancies, as evident from the PL analysis.
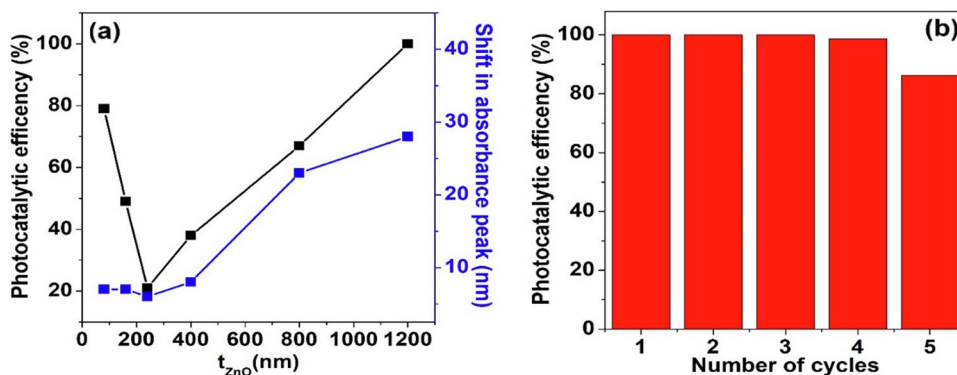
3.5 Photocatalytic studies

The photocatalytic activity of ZnO films was evaluated under UV–visible light illumination by using 0.5 mM RhB aqueous solution as an analyte. The dye solution was dropped uniformly on the surface of the ZnO photocatalyst and then the absorbance spectra were recorded at different illumination times. Electrons and holes are generated in the ZnO photocatalyst under light illumination which participates in the photocatalytic process. The decrease in absorbance after light illumination indicates the photocatalytic activity of ZnO thin films. The enhancement of photocatalytic activity is due to the number of photons absorbed and active centres on the surface of the catalyst [18, 37–39]. Generally, the photocatalytic efficiency is estimated using the following equation:

$$Photocatalytic\ efficiency = (A_0 - A_t)/A_0 * 100 \qquad (5)$$

where 'A_0' and 'A_t' are the peak values of absorbance before and after illumination. The decrease in the absorbance peak concerning light illumination illustrates the photodecolorization process of RhB molecule due to the destruction of its chromophore aromatic rings while the blue shift in the absorbance peak of RhB dye indicates the photodegradation of the dye molecules due to the de-ethylation process and hence the formation of RhB intermediaries [18, 39]. The variation in the photocatalytic efficiency of ZnO films as a function of t_{ZnO} is plotted in Fig. 7a and is found to be maximum at $t_{ZnO} = 1200$ nm.

The photocatalytic efficiency is found to be increased with an increase in t_{ZnO}(240–1200 nm). Similarly, the blue shift in the absorbance peak of RhB is depicted as a function of t_{ZnO} in Fig. 7a and this shift is also found to be maximum at $t_{ZnO} = 1200$ nm suggesting a higher photodegradation of RhB dye molecules. It is observed that the photodecolourization

Fig. 7 **a** Photocatalytic efficiency and shift in absorbance peak of RhB dye as a function of t_{ZnO} and **b** Reusability test of ZnO photocatalyst

Table 4 Time dependence study of ZnO photocatalyst

Time (min)	Photocatalytic efficiency (%)	Shift in RhB absorbance peak (nm)
5	20	6
10	70	10
15	100	28

process dominates at $t_{ZnO} \leq 400$ nm while the photodegradation phenomenon dominates at $t_{ZnO} > 400$ nm. The higher photocatalytic activity at $t_{ZnO} = 1200$ nm can be attributed to the synergistic effect due to the higher aspect ratio as observed from SEM analysis, lower bandgap energy, the higher concentration of oxygen vacancies as evident from the PL analysis as well as due to the enhanced photo-generation of charge carriers as evident from the I-V characteristics. In this work, the particle size (both crystallite size from XRD analysis and grain size from SEM analysis) is found to increase with t_{ZnO}. According to Tan et al., the formation of a thicker space charge layer (SCL) in larger particles is responsible for an increased band bending which aids the charge carrier separation [24]. A comparatively smaller space layer and lower band bending are observed in small-sized particles, but they exhibit better inter-particle contact leading towards good charge transport. Since the particle size and density increases with t_{ZnO}, the photogeneration and separation of charge carriers will also increase as evident from photocurrent studies given in Fig. 5. We have also observed that the band gap energy decreases with t_{ZnO} and found to be lower at $t_{ZnO} = 1200$ nm. A smaller band gap favours the photogeneration of charge carriers and hence improves the photocatalytic activity [15].

A comparison between Figs. 6 and 7a clearly shows a direct relationship between the photosensitivity and photodegradation of RhB molecules. Since the optimum efficiency is obtained at $t_{ZnO} = 1200$ nm, the time-dependent photocatalytic activity of ZnO film was also studied and is depicted in Table 4. Furthermore, the reusability test of the ZnO thin film photocatalyst is shown in Fig. 7b. It exhibited good reusability and stability up to four cycles. A high stability, reusability and efficiency are essential for a material to be used as a photocatalyst [31]. Thus, this work highlights the photocatalytic and photocurrent properties of ZnO thin films for various device applications.

4 Conclusions

A cost-effective ZnO thin film was fabricated via ultrasonic spray pyrolysis technique. XRD patterns exhibited the formation of polycrystalline wurtzite phase of ZnO. SEM images showed the formation of nanorod structure with uniform distribution of grains. The photocurrent and photocatalytic properties of ZnO thin films were studied as a function of its film thickness (t_{ZnO}). The ZnO film with $t_{ZnO} = 1200$ nm showed a higher aspect ratio and lower bandgap energy favouring the photocatalytic and photocurrent properties. Higher generation and separation of photogenerated charge carriers at $t_{ZnO} = 1200$ nm were confirmed by the improved photosensitivity as well as a higher concentration of oxygen vacancies from I-V characteristics and photoluminescence analysis respectively. The incident photon-to-electron conversion efficiency (IPCE) for the ZnO film with $t_{ZnO} = 1200$ nm was estimated to be 31.5%. Furthermore, the photocatalytic efficiency, as well as the photodegradation mechanism, was found to be maximum at $t_{ZnO} = 1200$ nm. The ZnO photocatalyst exhibited 100% efficiency with good stability and reusability. Thus, this work explored the photocatalytic and photocurrent properties of ZnO thin films and observed a direct correlation between the photosensitivity parameter and the photodegradation of RhB dye molecules.

Author contributions KCS and KK designed the work. SI and KVA performed the experiments. JPB, SS, KK and SI analysed the results. SI, KVA, MBL wrote Ist draft of manuscript. All authors read and approved the final manuscript.

Data availability The data collected from the respondents are available with the corresponding author and may be provided upon reasonable request.

Declarations

Competing interests The authors declare no competing interests.

References

1. Vyas S. ZnO as a promising material for applications in electronics, optoelectronics, biomedical and sensors. Johnson Matthey Technol Rev. 2020;64:202.
2. Sugumaran S, Ahmad MNB, Jamlos MF, Bellan CS, Pattiyappan S, Rajamani R, Rathis KS. Transparent with wide band gap InZnO nano thin film: preparation and characterizations. Opt Mater. 2015;49:348.
3. Ong CB, Ng LY, Mohammad AW. A review of ZnO nanoparticles as solar photocatalysts: synthesis, mechanisms and applications. Renew Sust Energ Rev. 2018;81:536.
4. Chen Y. 2018. Review of ZnO Transparent Conducting Oxides for solar applications.Mater. Sci. Eng. *C*423 012170.
5. Saravanan R, Gupta VK, Narayanan V, Stephen A. Comparative study on photocatalytic activity of ZnO prepared by different methods. J Mol Liq. 2013;181:133–41.
6. Uribe-Lopez M C, Hidalgo-Lopez M C, Lopez-Gonz R, Frías-Marquez D M, Núñez-Nogueira G, Hernandez-Castillo D and Alvarez-Lemus M A, Journal of Photochemistry & Photobiology, A: Chemistry, 2021; 404 112866
7. Kaneva N, Stambolova I, Blaskov V, Dimitriev Y, Bojinova A, Dushkin C. A comparative study on the photocatalytic efficiency of ZnO thin films prepared by spray pyrolysis and sol-gel method. Surf Coat Technol. 2012;207:5–10.
8. Klauson D, Gromyko I, Dedova T, Pronina N, Krichevskaya M, Budarnaja O, OjaAcik IO, Volobujeva O, Sildos I, Utt K. Study on photocatalytic activity of ZnO nanoneedles, nanorods, pyramids and hierarchical structures obtained by spray pyrolysis method. Mater Sci Semicond Process. 2015;31:315–24.
9. Chen X, Wu Z, Liu D, Gao Z. Preparation of ZnOPhotocatalyst for the efficient and rapid photocatalytic degradation of Azo dyes. Nanoscale Res Lett. 2017;12:143.
10. de León JAG, Centeno AP, Rosas GG, Camps E, Arias-Ceró JS, Santana-Aranda MA, Quiñones-Galvan JG. ZnO thin films grown at different plasma energies by the laser ablation of metallic Zn with a 532 nm wavelength. MateR Res Express. 2020;7:016423.
11. Cho J, Hwang S, Chung S, Ko DH, Chung S. Transparent ZnO thin-film deposition by spray pyrolysis for high-performance metal-oxidefield-effect transistors. Materials. 2019. https://doi.org/10.3390/ma12203423.
12. Park YK, Choi YK, Kim HS, Kim JH, Hahn JH, Hahn YB. High performance field-effect transistors fabricated with laterally grown ZnO nanorods in solution. Nanotechnolog. 2011;22:185310.
13. Rahal H, KihalR AAM, GhersM FD. Electrodeposition and characterization of ZnO thin films using sodium thiosulfate as an additive for photovoltaic solar cells. J Semicond. 2017;8:053002.
14. Bahtiar A, Saragi T, Hidayat S, Safriani L. ZnO thin films prepared using the ultrasonic spray pyrolysis method for high performance metal oxides-based photoconductors. Key Eng Mater. 2020;860:274.
15. Bakhtiarniaa S, Sheibania S, Billard A, Sunc H, Aubry E, Yazdi MAP. Enhanced photocatalytic activity of sputter-deposited nanoporous $BiVO_4$ thin films by controlling film thickness. J Alloy Compd. 2021;879:160463.
16. Pinaud BA, Vesborg PCK, Jaramillo TF. Effect of film morphology and thickness on charge transport in Ta_3N_5/Ta photoanodes for solar water splitting. J Phys Chem C. 2012;116:15918–24.
17. Zhang HZ, Sun XC, Wang RM, Yu DP. Growth and formation mechanism of c-oriented ZnO nanorod arrays deposited on glass. J Cryst Growth. 2004;269:464.
18. Jayakrishnan AR, Alex KV, Tony A, Kamakshi K, Silva JPB, Shiva Prasad M, Sekhar KC, Gomes MJM. Barium-doped Zinc Oxide thin films as highly efficient and reusable photocatalysts. ChemistrySelect. 2020;5:2824.
19. Roza L, Fauzia V, Rahman MYA. Tailoring the active surface sites of ZnO nanorods on the glass substrate for photocatalytic activity enhancement. Surf Interfaces. 2019;15:117–24.
20. Perez AF, Casado VR, Solis TV, Marba G. Room temperature sintering of polar ZnO nanosheets: II-mechanism. Phys Chem. 2017;15:16413.
21. Leelavathi A, Madras G, Ravishankar N. Origin of photocatalytic activity and photocondution in high aspect ratio ZnO nanorods. Phys Chem Chem Phy. 2013;15:10795–802.
22. Yang XD, Su SC, Xu Y, Mei T. Effect of thickness on the structural, electrical and optical properties of ZnO films deposited by MBE. Adv Mat Res. 2011;311:1271.
23. Mridha S, Basak D. Effect of thickness on the structural, electrical and optical properties of ZnO films. Mater Res Bull. 2007;42:875.
24. Tan HL, Amal R, Ng YH. Exploring the different roles of particle size in photoelectrochemical and photocatalytic water oxidation on BiVO. ACS Appl Mater Interfaces. 2016;8:28607.
25. Sugumaran S, Bellan CS. A Novel InTiO thin film by thermal evaporation technique for high mobility/conductivity with tunable visible emissions. Optik. 2019;185:997.

26. Wang YG, Lau SP, Lee HW, Yu SF. Photoluminescence study of ZnO films prepared by thermal oxidation of Zn metallic films in air. J Appl Phys. 2003;94:354.
27. Aguilar GV, Jaime Fonseca MR, Ramírez AM, JuárezGracia AG. Photoluminescence studies on ZnO thin films obtained by sol-gel method. Recent Appl Sol-Gel Synth. 2017;10:195.
28. Sugumaran S, Bellan CS, Bheeman D. Thermally evaporated InZnO transparent thin films: optical, electrical and photoconductivity. Opt Mater. 2017;72:618.
29. Zahedi F, Dariani RS, Rozati SR. Structural, optical and electrical properties of ZnO thin films prepared by spray pyrolysis: effect of precursor concentration. Bull Mater Sci. 2014;37:433.
30. Kim D, Leem J. Transparent and flexible ZnOnanorods induced by thermal dissipation annealing without polymer substrate deformation for next-generation wearable devices. RSC Adv. 2021;11:17538.
31. Gonzailez AEJ, Nair PK. Photosensitive ZnO thin films prepared by the chemical deposition method SILAR. Semicond Sci Technol. 1995;10:1277.
32. Mridha S, Basak D. Thickness dependent photoconducting properties of ZnO films. Chemical Phys Lett. 2014;427:62.
33. Lv P, Lin L, Zheng W, Zheng M, Lai F. Photosensitivity of ZnO/Cu_2O thin film heterojunction. Optik. 2013;124:2654.
34. Mirdha S, Basak D. Effect of thickness on the structural, electrical and optical properties of ZnO films. Mater Res Bull. 2007;124:2654.
35. Chen Z, Deutsch TG, Dinh HN, Domen K, Emery K, Forman AJ, Gaillard N. Incident photon to current efficiency and photocurrent spectroscopy. Photoelectrochemical Water Splitting. New York: Springer; 2013.
36. Palma G, Cozzarini L, Capria E, Morgera AF. A homemade system for IPCE measurement of standard and dye sensitized solar cell. Rev Sci Instrum. 2015;86:013112.
37. Sugumaran S, Bellan CS, Devaraj N. Novel mixed cubic-rutile structured In_2O_3-TiO_2 composite nanoparticles (InTiO CNPs): structure, morphology, photoluminescence and photocatalyticactivity. Optik. 2018;174:15.
38. Alex KV, Jayakrishnan AR, Sulthan Ibrahim A, Kamakshi K, Silva JPB, Sekhar KC, Gomes MJM. Substrate temperature induced effect on microstructure, optical and photocatalytic activity of ultrasonic spray pyrolysis deposited MoO_3 thin films. Mater Res Exp. 2019;6:066421.
39. Alex KV, Arya P, Jayakrishnan AR, Kamakshi K, Silva JP, Sekhar KC. Charge coupling enhanced photocatalytic activity of $BaTio_3$/MoO_3heterostructures. ACS Appl Mater Interfaces. 2019;11:40114.